AUTHOR(S)
Ohshima, M., Moriguchi, T., Enmi, J., Kawashima, H., Koshino, K., Zeniya, T., Tsuji, M., & Iida, H.

TITLE
[123I]CLINDE SPECT as a neuroinflammation imaging approach in a rat model of stroke

YEAR
2024

DOI
10.1016/j.expneurol.2024.114843

CITATION
Ohshima, M., Moriguchi, T., Enmi, J., Kawashima, H., Koshino, K., Zeniya, T., Tsuji, M., & Iida, H. (2024). [123I]CLINDE SPECT as a neuroinflammation imaging approach in a rat model of stroke. *Experimental Neurology*, 378, 114843. https://doi.org/10.1016/j.expneurol.2024.114843

VERSION
Accepted Manuscript

Title: ^{123}I CLINDE SPECT as a neuroinflammation imaging approach in a rat model of stroke.

Authors

Makiko Ohshima[a,c*], Tetsuaki Moriguchi[b,d], Jun-ichiro Enmi[b,e], Hidekazu Kawashima[b,f], Kazuhiro Koshino[b,g], Tsutomu Zeniya[b,h], Masahiro Tsuji[a,i], Hidehiro Iida[b,j]

Authors' affiliation

[a]Department of Regenerative Medicine and Tissue Engineering, National Cerebral and Cardiovascular Center, 6-1 Kishibe-Shimmachi, Suita, Osaka, 564-8565, Japan

[b]Department of Investigative Radiology, National Cerebral and Cardiovascular Center, 6-1 Kishibe-Shimmachi, Suita, Osaka, 564-8565, Japan

(Current authors' affiliation)

[c]Department of Neurobiology, Care Sciences & Society, Karolinska Institute, Visionsgatan 4, Solna, 171 64, Sweden

[d]Institute of Physics, University of Tsukuba, Ibaraki, 305-8571, Japan

[e]Graduate School of Frontier Biosciences, Osaka University, 1-3 Yamadaoka, Suita, Osaka, 565-0871, Japan

[f]Radioisotope Research Center, Kyoto Pharmaceutical University, 1 Misasagi-Shichono-cho, Yamashina-ku, Kyoto, 607-8412, Japan

[g]Department of Systems and Informatics, Hokkaido Information University, 59-2 Nishi-nopporo Ebetsu, Hokkaido, Japan

[h]Graduate School of Science and Technology, Hirosaki University, 3 Bunkyo-cho, Hirosaki, Aomori, 036-8561, Japan

[i]Department of Food and Nutrition, Kyoto Women's University, 35 Imakumano, Kitahiyoshi-cho, Higashiyama-ku, Kyoto, 605-8501, Japan

[j]Faculty of Medicine, University of Turku, and Turku PET Centre, Turku University Hospital, Kiinamyllynkatu 4-8, 20520 Turku, Finland

Corresponding author: Makiko Ohshima, Ph.D.

Department of Regenerative Medicine and Tissue Engineering, National Cerebral and Cardiovascular Center, 6-1 Kishibe-Shimmachi, Suita, Osaka, 564-8565, Japan

(Current) Department of Neurobiology, Care Sciences & Society, Karolinska Institute, Visionsgatan 4, Solna 171 64, Sweden

Tel: +46-76-576-8727

E-mail addresses: makiko.ohshima@ki.se

Running title

^{123}I CLINDE SPECT imaging in rat model of stroke

Abstract

Poststroke neuroinflammation exacerbates disease progression. [^{11}C]PK11195-positron emission tomography (PET) imaging has been used to visualize neuroinflammation; however, a short half-life (20 min) of [^{11}C]PK11195 limit its clinical use. [^{123}I]CLINDE has a longer half-life (13 h); therefore, [^{123}I]CLINDE is potentially more practical than PK11195-PET imaging, particularly with improved image reconstruction technologies in single-photon emission computed tomography (SPECT) imaging. The objective of this study was to 1) validate neuroinflammation imaging by [^{123}I]CLINDE and 2) to investigate the mechanisms underlying stroke in association with neuroinflammation using multimodal techniques including MRI, gas-PET, and histological analysis in a rat model of ischemic stroke, i.e., permanent middle cerebral artery occlusion (pMCAo). [^{123}I]CLINDE-SPECT images at 6 days post pMCAo significantly corresponded to immunohistochemical images stained with CD68 antibody (marker for microglia/macrophages), similar to the level of [^{11}C]PK11195-PET images. Also, [^{123}I]CLINDE-SPECT images well corresponded to autoradiography images. Rats with severe infarct defined by MRI exhibited neuroinflammation in the peri-infarct area and less neuroinflammation in the ischemic core accompanied by a moderate reduction in cerebral metabolic rate of oxygen ($CMRO_2$) in ^{15}O-gas-PET. Rats with moderate to mild infarct exhibited neuroinflammation in the ischemic core. This study demonstrates that [^{123}I]CLINDE-SPECT imaging is suitable for neuroinflammation imaging, and that distribution of neuroinflammation varies depending on the severity of infarction.

(204 words)

Key words

CLINDE, PK11195, Microglia, inflammation imaging, stroke, middle cerebral artery occlusion, SPECT, PET, oxygen consumption

Abbreviations

PET: positron emission tomography

SPECT: single-photon emission computed tomography

pMCAo: permanent middle cerebral artery occlusion

$CMRO_2$: cerebral metabolic rate of oxygen

TSPO: Translocator protein

Introduction

Stroke is the second leading cause of death and disability worldwide, i.e., the second leading cause of global disability-adjusted life-years (DALYs) in patients over age 50 (Diseases and Injuries, 2020). As treatments of acute ischemic stroke, current guidelines recommend intravenous thrombolysis, e.g., intravenous administration of tissue plasminogen activator (tPA), and endovascular thrombectomy (Powers et al., 2019). Therapeutic time windows for those treatments are short; tPA has a 4.5 h time window, and thrombectomy has a up to 24 h time window in a subset of well-selected patients (Jadhav et al., 2021), following ischemic stroke onset. This short therapeutic time windows, along with several other reasons, result in a situation, in which large majority of potentially eligible patients cannot receive those acute therapies (Bambauer et al., 2006). Even if patients can receive the acute treatments, the rate of complete recanalization and the outcome of the patients are far from satisfactory (Saqqur et al., 2007). Therefore, simple and effective treatments with long-therapeutic time window are needed to improve outcome of stroke patients.

In recent decades, a number of studies have reported that poststroke inflammation is integral to disease outcome, and therapeutic approaches aimed at promoting anti-inflammatory responses in ischemic

stroke have been tested both experimentally and clinically (Dirnagl et al., 1999) (Drieu et al., 2018) ((Lambertsen et al., 2019). Compared with intravenous thrombolysis and endovascular thrombectomy, anti-inflammatory treatments have longer therapeutic time windows. Currently, however, there are no anti-inflammatory drugs for stroke treatment proven effective by large-scale randomized control trials. The progression, intensity, extent, and resolution of inflammation in the brain vary depending on the patient. To better understand the pathophysiology of neuroinflammation in patients with acute ischemic stroke, noninvasive imaging for neuroinflammation is required. In the future, to select patients for anti-inflammatory treatment and to modify the treatment timing, neuroinflammation imaging may become required at hospitals. Positron emission tomography (PET) and single-photon emission computed tomography (SPECT) are applicable evaluation tools for neuroinflammation imaging in clinical practice.

Computed tomography (CT) and magnetic resonance imaging (MRI) have been used as a noninvasive imaging technique in stroke to allow physicians to decide the treatment plan. However, the outcome of each patient does not always reflect early evaluation with CT and/or MRI (Gonzalez, 2012). Inflammation in the brain in the subacute phase exacerbates ischemic infarction. The intensity, time course and localization of inflammation are different from patient to patient, which leads to large variability in the resulting ischemic infarct. Hence, better imaging technique for neuroinflammation is needed to improve accuracy of disease prediction and the outcome of stroke patients.

Translocator protein (TSPO) is a five-transmembrane domain protein localized in mitochondria in immune cells, such as macrophages in peripheral tissues and microglia in the central nervous system and expressed in very low concentrations in normal brain (Cumming et al., 2018). TSPO is expressed in activated microglia cells and upregulated in response to brain damage. The use of a TSPO ligand is a mainstream approach for neuroinflammation imaging and used in a variety of neurological disease models (Crawshaw and Robertson, 2017) (Shimochi et al., 2022). Most inflammation tracers for PET target TSPO ligands; to date, many such tracers have been developed (e.g., [^{11}C]PBR28, [^{11}C](R)-PK11195, [^{18}F]PBR111, [^{18}F]DPA714). However, the half-lives of the radioisotopes used in these PET tracers are

very short (e.g., 20 min for ^{11}C and 2 hours for ^{18}F). The binding affinity of each tracer varies, and the specificity for the detection of inflammation is under investigation; therefore, further verification and use of tracers with longer half-lives are required to apply neuroinflammation imaging to clinical practice ((Cumming et al., 2018)). Recently, [^{123}I]CLINDE has been characterized as a SPECT tracer of inflammation; permeability through blood-brain-barrier into the brain and specificity for TSPO binding have been demonstrated in several disease models in animals (Mattner et al., 2008). The long half-life of [^{123}I]CLINDE (13 h) is beneficial for clinical use. Moreover, SPECT is widely used in clinical practice than PET.

The purpose of this study was 1) to validate [^{123}I]CLINDE-SPECT as a neuroinflammation imaging by using immunohistochemistry with a microglia marker and autoradiography, and to compare with [^{11}C]PK11195-PET, and 2) to investigate the mechanisms underlying ischemic stroke in association with neuroinflammation using multimodal techniques including MRI, gas-PET, and histological analysis in a rat model of ischemic stroke, i.e., permanent middle cerebral artery occlusion (pMCAo).

Material and Methods

Permanent middle cerebral artery occlusion (pMCAo)

All animal experiments were performed in accordance with protocols approved by the Experimental Animal Care and Use Committee of the National Cerebral and Cardiovascular Center in Osaka Japan. We used pMCAo model, which is more relevant to the pathophysiology of patients without acute thrombolysis and/or thrombectomy. The Stroke Therapy Academic Industry Roundtable (STAIR) guideline is the best-known guideline for preclinical studies in this field (Stroke Therapy Academic Industry, 1999). The guideline emphasizes the importance of using pMCAo models in preclinical studies, although majority of preclinical studies have been conducted in transient MCAo models ((McBride and Zhang, 2017)). A total of 17 9- to 11-week-old male Sprague–Dawley (SD) rats (Japan SLC Inc., Hamamatsu, Japan) were

subjected to pMCAo using an intraluminar suture method based on the Koizumi model (Memezawa et al., 1992). For Experiment 1 (Exp. 1), 9 rats with pMCAo were subjected to MRI/PET/SPECT imaging followed by immunohistochemical analysis (Fig 1A). For Experiment 2 (Exp. 2), 8 rats with pMCAo were subjected to MRI followed by autoradiography analysis (Fig 1A). Briefly, under isoflurane anesthesia (4% for induction and 1-2% for maintenance), the left external carotid artery (ECA) was exposed following a cervical median incision, and a notch was made at a 2-mm position from the carotid bifurcation to the periphery. A 4-0 nylon suture coated with dental impression material (Provil® novo Light, Heraeus, Germany) at the tip was inserted through the notch site. The tip of the suture remained at the proximal end of the anterior cerebral artery to block blood flow into the MCA. The incision site of the ECA was closed, and the incision of the neck was sutured. Four 8-week-old male SD rats were prepared as controls in Exp. 2 (Fig. 1A).

MRI

On Day 3 or 4 after pMCAo surgery, rats were anesthetized with isoflurane and placed in a prone position, and their heads were secured with a bite bar and ear bars. All MRI scans were performed using a 7-T horizontal bore imaging system (BioSpec 70/30 USR, Bruker BioSpin, Germany) equipped with a gradient system capable of a maximum gradient amplitude of 669 mT/m and a slew rate of 7989 T/m per second. Radiofrequency transmission was performed by using an 86-mm ID volume coil. The signal was detected by a 4-channel receive-only phased-array surface coil. T2-weighted (T2W) images were acquired using a rapid acquisition with relaxation enhancement (RARE) sequence with the following parameters: RARE factor, 8; repetition time (TR)/echo time (TE), 14000/20 msec; number of averages, 2; matrix size, 160×160; field of view (FOV), 3.2×3.2 cm^2; in-plane spatial resolution, 200×200 μm^2; slice thickness, 0.5 mm; gapless; number of slices, 70; and scan time, 9 min 20 sec. Three-dimensional (3D) time-of-flight (TOF) magnetic resonance angiography (MRA, Fig. 1B) images were acquired by a fast low-angle shot sequence with the following parameters: TR/TE, 22.0/2.9 msec; number of averages, 1; matrix size,

200×200×200; FOV, 3.2×3.2×3.52 cm^3; spatial resolution, 160×160×160 μm^3; and scan time, 9 minutes. In 3D TOF MRA, a tilted optimized nonsaturating excitation pulse and flow compensation were used. Maximum intensity projection images were reconstructed using AZEWIN software (AZE, Ltd, Japan). In Exp. 1, MRI scans were repeated on Day 8 ± 1 again (Fig. 1A). Severity was defined as the infarct volume ratio per cerebral hemisphere volume. The infarct area and cerebral hemisphere area every 2 mm from 2-14 mm from the frontal pole on T2W images were measured by ImageJ (NIH, USA). Also, the infarct area and cerebral hemisphere area were summed to determine the infarct volume ratio per cerebral hemisphere volume.

[^{11}C]PK11195-PET scanning

We conducted [^{11}C]PK11195-PET and [^{123}I]CLINDE-SPECT at On Day 6 ± 1 post pMCAo as studies with PET/SPECT show that activated microglia are detected from a few days to a few weeks, with a maximum at 7-14 days following ischemic insults ((Rojas et al., 2007; Zinnhardt et al., 2015)). In each rat, both [^{11}C]PK11195-PET and [^{123}I]CLINDE-SPECT scanning were performed on the same day.

The precursor (R)-N-desmethyl PK11195 was obtained commercially from NARD Institute Ltd. (Hyogo, Japan), and [^{11}C]PK11195 was synthesized by a conventional method using [^{11}C]CH3I as the methylation agent(Shah et al., 1994). On Day 6 ± 1 post pMCAo in Exp. 1, rats were anesthetized with 1-2% isoflurane and [^{11}C]PK11195 (Fig. 1 C) (28.6-240.6 MBq in 0.1 mL saline) was administered to rats via their tail veins. PET scanning with a Micro PET Focus 120 (8 cm bore; axial FOV of 8 cm; 1.0 mm FWHM, CTI/Siemens, SIEMENS Health care USA Inc.) was performed for 60 min after [^{11}C]PK11195 administration.

[^{123}I]CLINDE-SPECT scanning

[^{123}I]CLINDE (Fig. 1D) was purchased from MAP Medical Technologies Oy (Finland). On the same day that [^{11}C]PK11195-PET was performed (= Day 6 ± 1 post pMCAo), rats were anesthetized with 1-2% isoflurane, and [^{123}I]CLINDE (19.2-41.9 MBq in 1.0 mL) was administered to the rats via their tail veins after 4 min of CT scanning using a four-headed multipinhole NanoSPECT/CT (Bioscan Inc., Washington DC, USA). SPECT scanning was performed for 90 min after the administration of [^{123}I]CLINDE. Each head of the NanoSPECT/CT was equipped with a tungsten-based nine-pinhole collimator. In this study, a rat aperture (aperture 5), which comprises a total of 36 individual 1.5-diameter pinholes (nine pinholes in every collimator, 4 × 9 = 36), provides a maximum resolution ≤ 1.25 mm, a maximum sensitivity > 1000 cps/MBq and a cylindrical FOV of 60 mm × 24 mm (diameter × length) for SPECT imaging. The energy window was centered at 159 keV with a window width of ± 10%. SPECT images were reconstructed by an ordered subset expectation maximization (OSEM) iteration algorithm dedicated to multipinhole reconstruction.

Image processing and data analyses

Time-activity curves (TACs) from each hemisphere were obtained from dynamic PET/SPECT images, and the activities were calculated as kBq/mL/injected dose (ID) in regions of interest (ROIs) set over the center of the hemisphere, as shown in Figure 1E (*c*: MCA region), at both the striatal and hippocampal levels. To reconstruct scanning images, the volumes of interest (VOIs) (11 slices × 0.5 mm-thick) were integrated by the same ROI. The average distribution volume of [^{11}C]PK11195 or [^{123}I]CLINDE in the VOI in the contralateral hemisphere was defined as 1. The registration images were generated by integrating PET images every 30 sec for 30 min from 30 min post-[^{11}C]PK11195 administration or SPECT images every 10 min for 60 min from 30 min post-[^{123}I]CLINDE administration. For data analyses, ROIs were placed as shown in Figure 1E; striatum (*a*), cortex (*b*), MCA region (*c*), and mean radioactivity in the ROIs were analyzed using Qview software (Molecular Imaging Labo Inc.,

Japan). For the definitions of terms used in this study, the MCA territory including striatum, cortex and partially hippocampus was defined as the MCA region (*c* in Fig. 1E).

^{15}O-gas PET scanning

To produce ^{15}O-labeled gases, $^{15}O_2$ and $C^{15}O_2$ were continuously added into 300 mL 80% N_2 and 20% O_2 at 1.0 GBq/min over 15 min, and $C^{15}O$ was continuously added into 300 mL 80% N_2 20% O_2 at 1.0 GBq/min for 4 min, as previously reported (Temma et al., 2017). On Day 7 ± 1 post pMCAo in Exp. 1, the heads of rats were secured with a plastic holder with a fabric face mask inside of it; then, rats were anesthetized by inhalation of 1-2% isoflurane mixed with ^{15}O-labeled gases during PET scanning. Air inside of the holder was continuously circulated at 10 L/min to keep extra ^{15}O-labeled gases out. PET scans were performed during continuous inhalation of $C^{15}O_2$ and $^{15}O_2$ and then at 11 min after the start of $C^{15}O$ inhalation by Micro PET Focus 120 (8 cm bore; axial FOV of 8 cm; 1.0 mm FWHM, CTI/Siemens, SIEMENS Healthcare USA Inc.). The dynamic images were integrated over 8 min from the start of the scan for $C^{15}O_2$ and $^{15}O_2$ and over 6 min for $C^{15}O$. The obtained build-up phase images of $C^{15}O_2$, $^{15}O_2$, and $C^{15}O$ were defined as cerebral blood flow (CBF), cerebral metabolic rate of oxygen ($CMRO_2$) and cerebral blood flow volume (CBV) images, respectively.

Immunohistochemistry

To validate [^{123}I]CLINDE and [^{11}C]PK11195 as neuroinflammation tracers, the distribution of [^{123}I]CLINDE and [^{11}C]PK11195 in the infarct areas was compared with the accumulation of CD68-positive microglia in the infarct areas. Rats were transcardially perfused with saline with 1 U/ml heparin followed by fixation with 4% paraformaldehyde buffered with saline (PFA). Brains were removed and fixed in 4% PFA overnight. Brain tissues were cut coronary to 2 mm blocks, embedded in paraffin blocks,

and cut into 2 μm sections. After deparraffinization, the sections were treated with Protein Block (Dako Cytomation, Glostrup, Denmark) and incubated with mouse anti-rat CD68 (clone ED-1; Millipore, Bedford, MA, 1:100) in diluents (DAKO Cytomation) overnight at 4 °C. The next day, the CD68 antibodies were labeled with horseradish peroxidase (HRP) by incubation with anti-mouse secondary antibody (LSAB/HRP kit, Dako Cytomation) for 30 min. CD68-positive cells were visualized with 0.5% diaminobenzidine (Dako Cytimation) and 0.03% hydrogen peroxide. Nuclei were stained with hematoxylin. Whole areas in striatal sections 2-4 mm from the frontal pole and hippocampal sections 6-8 mm from the frontal pole were photographed using a digital microscope (BIOREVO BZ-9000; KEYENCE, Japan). The CD68-positive area (/mm^2) was measured using image-processing software (WinROOF, Mitani Co. Ltd., Japan). The striatal- and hippocampal-level [^{123}I]CLINDE and [^{11}C]PK11195 images and immunohistochemistry images were analyzed for correlation analysis.

Autoradiography

On Day 6 ± 1 post pMCAo in Exp. 2, rats were anesthetized with 1-2% isoflurane and [^{123}I]CLINDE (8.87-22.4 MBq in 1.0 mL) was administered to rats via their tail veins. Rats were transcardially perfused with saline with 1 U/ml heparin followed by fixation with 4% PFA. Brains were removed, fixed in 4% PFA overnight, cut coronary in 2 mm intervals from the tips of the brains through the whole brain. The brain tissues were transferred into 30% sucrose in PBS, embedded in OTC compound (Sakura Finetek USA, Inc., CA, USA), and frozen in liquid nitrogen. The coronal sections were sliced into 20 μm thick sections with a cryostat microtome and air dried at room temperature. The slices were placed in contact with an imaging plate (BAS IP MS-2025, Fujifilm Co., Japan) for 1 week, and autoradiograms were acquired using an image plate reader (BAS 5000, Fujifilm).

Statistical analysis

All data are presented as the mean ± standard deviation (SD). TACs were assessed using two-way repeated-measures ANOVAs followed by Bonferroni-Dunn tests. Pearson's regression analysis was employed to test the correlation. A probability value of < 0.05 was considered statistically significant. All statistical analyses were performed using Statcel3 software (OMS Ltd. Saitama, Japan).

Results

Validation of [^{123}I]CLINDE as a neuroinflammation tracer compared with immunohistochemistry images

MRA at Day 3 or 4 confirmed success of the pMCAo in all 9 rats subjected to the procedure in Exp. 1. The ipsilateral uptake of [^{11}C]PK11195 and [^{123}I]CLINDE at Day 6 significantly increased compared to the contralateral uptake at both the striatal and hippocampal levels (Fig. 2). Based on the TAC curves, PET images between 30 and 60 min post[^{11}C]PK11195 administration and SPECT images between 30 and 90 min post[^{123}I]CLINDE administration were integrated to generate images for analyses (Fig. 3). In the ipsilateral hemisphere, significant increases in [^{11}C]PK11195 and [^{123}I]CLINDE activities were detected in PE/SPECT images at both the striatal and hippocampal levels in all pMCAo rats. The distribution of [^{123}I]CLINDE was generally similar to that of [^{11}C]PK11195 in most animals, although there were some minor differences between them. Referring to the infarct area on T2W images on Day 8 and H&E-stained images on Day 9, the areas of high accumulation of either [123I]CLINDE or [11C]PK11195 radiotracer were found to be mainly at the infarct border (Fig. 3).

Actual microglial distribution in the infarct area was assessed in images of CD68-positive microglial staining at Day 9. In the comparison between the radiotracer-accumulated area and the CD68-positive area, the accumulation of both [^{11}C]PK11195 and [^{123}I]CLINDE was concordant with the CD68-positive area, which demonstrated that [^{11}C]PK11195 and [^{123}I]CLINDE selectively bound to activated microglia gathered in ischemic areas (Fig. 3). To investigate the sensitivity of [^{11}C]PK11195 and [^{123}I]CLINDE tracers quantitively, 3 ROIs for striatal level (*a* = striatum; *b* = cortex; *c* = MCA region in Fig. 1E) and for

hippocampal level (central area; cortex; MCA region) were set on [^{11}C]PK11195-PET, [^{123}I]CLINDE-SPECT and CD68 staining images. Of note, those three evaluations, i.e., PET, SPECT, and immunostaining, were performed in each one of the 9 rats, and PET and SPECT were performed on the same day. The ratios of the ipsilateral/contralateral side in each imaging method were calculated. The correlation between [^{123}I]CLINDE-SPECT imaging and CD68 staining (Fig. 4A) and the correlation between [^{11}C]PK11195-PET and CD68 staining (Fig. 4B) at the striatal level were analyzed. The best correlation with CD68 staining images were seen in the striatum in both [^{123}I]CLINDE-SPECT (p value = 0.046, R^2 = 0.46) and [^{11}C]PK11195 PET images (p value = 0.01, R^2 = 0.64), while the correlation was weaker in the cortex (*b* in the ROI) and MCA region (*c* in the ROI). There was no significant correlation between the radiotracer distribution in either [^{123}I]CLINDE-SPECT or [^{11}C]PK11195-PET images and the CD68-positive area at the hippocampal level. Taken together, [^{123}I]CLINDE-SPECT imaging well visualized distribution of neuroinflammation after stroke, and its accuracy was mostly similar to that of [^{11}C]PK11195-PET imaging.

Validation of [^{123}I]CLINDE with autoradiography images

[^{123}I]CLINDE autoradiography was performed to evaluate the validity of [^{123}I]CLINDE SPECT imaging. MRA on Day 3 or 4 confirmed success of the pMCAo in all 8 rats subjected to the procedure in Exp. 2. Infarct severity was determined by T2W images taken on Days 3 or 4. In a control rat, uptake of [^{123}I]CLINDE into brain tissue was not observed (Fig. 5). In a rats with a mild infarct (No. 10 in Fig. 5), [^{123}I]CLINDE accumulated markedly in the striatum and moderately in the cerebral cortex in the striatal slice, but hardly any accumulation was noted in the hippocampal slice. In a rat with a moderate infarct (No. 11 in Fig. 5), uptake of [^{123}I]CLINDE was observed over the MCA territory in both striatal and hippocampal slices. In a rat with a severe infarct (No. 12 in Fig. 5), the uptake of [^{123}I]CLINDE in the peri-infarct area (medial side of MCA territory) with the absence of uptake in most part of the striatum and overlying cortex was observed. Although the distribution patterns of [^{123}I]CLINDE varied depending

on the severity of infarcts, the patterns confirmed by autoradiography were reflected in [^{123}I]CLINDE-SPECT images (Fig. 6).

Severity of infarct were evaluated by the infarct volume in T2W MRI at Day 8 in Exp. 1. Individual animals were numbered from No. 1 to No. 9, and images of each animal are displayed in an order from most severe (left) to mildest (right) in Fig. 6. In a rats with a mild infarct (No. 9 in Fig. 6), [^{123}I]CLINDE accumulated markedly in the striatum and mildly in the cortex, which was similar to the autoradiography in the mild case (No. 10 in Fig. 5). In rats with a moderate infarct (No. 6-8 in Fig. 6), [^{123}I]CLINDE accumulated both the striatum and overlying cortex, which was similar to the autoradiography in the moderate case (No. 11 in Fig. 5). In rats with a severe infarct (No. 1-5 in Fig. 6), except for No. 2, [^{123}I]CLINDE accumulated markedly in the peri-infarct area (medial side of MCA territory) with less accumulation in most part of the striatum and overlying cortex, which was similar to the autoradiography in the severe case (No. 12 in Fig. 5). Such trends were also observed in immunohistochemistry with CD68 antibody. Taken together, the SPECT images accurately reflected the radioactive signal from [^{123}I]CLINDE. Importantly, the overall intensity of neuroinflammation, i.e., uptake of the tracer, across ipsilateral hemisphere did not corelate with infarct severity, but rather the distribution pattern of neuroinflammation corelated with infarct severity.

Dynamics of neuroinflammation and oxygen consumption corresponding to infarction in the pMCAo model.

Corresponding to the infarct area shown in T2W images on Day 8, reduction of CBF and $CMRO_2$ in the infarct area were observed by ^{15}O-gas PET on Day 6, and the degree of reduction was mostly severity-dependent. The reduction in $CMRO_2$ at striatum level correlated with the severity of infarct measured on T2W images (p value = 0.024, R^2 = 0.54). On the other hand, CBV was not altered by pMCAo regardless of the infarct severity (Fig. 6). For animals with moderate to mild infarction determined by MRI (i.e., No.

6-9 in Fig. 6), the reductions in the $CMRO_2$ were mild, but widespread substantial neuroinflammation in the MCA territories was observed in the [^{123}I]CLINDE-SPECT images. For animals with severe infarction (i.e., No. 1-5 in Fig. 6), substantial reductions in the $CMRO_2$ were observed, and neuroinflammation was mostly confined to border area of infarction, where the reductions of $CMRO_2$ were relatively mild. Taken together, the accumulation of neuroinflammation tracers was observed in the area where oxygen was metabolized by cells but not in the area where the blood supply was severely blocked, and oxygen was not metabolized by cells. Of note, Fig. 6 demonstrates that [^{123}I]CLINDE-SPECT images tended to have higher spatial resolution and higher contrast than [^{11}C]PK11195-PET images.

(1,098 words)

Discussion

In this study, we demonstrated that 1) [^{123}I]CLINDE-SPECT was generally of comparable quality to [^{11}C]PK11195-PET as neuroinflammation imaging, and 2) the distribution pattern, rather than overall intensity, of neuroinflammation corelated with infarct severity, and the distribution pattern also corelated with $CMRO_2$.

In addition to TSPO, there are other molecular targets for microglial imaging, such as GSK3, ROS, COX1, COX2, and SIP1. Radioactive tracers corresponding to these targets have been developed (i.e., [^{11}C]PF-367 for GSK3, [^{11}C]hydromethidine for ROS, [^{11}C]PSI3 for COX1, [^{11}C]MCI for COX2, and [^{18}F]TZ43113 for SIP1) (Narayanaswami et al., 2018). Those tracers have some limitations. For instance, COX1 is expressed in the hippocampal area only under inflammatory stimuli (Narayanaswami et al., 2018). In ischemic stroke, ROS (reactive oxygen species) production reaches a peak in a short time in the acute phase (Olmez and Ozyurt, 2012), and imaging targeting ROS is limited to a short time window (< 10 hours postonset) ((Abe et al., 2015)). Imaging broad inflammation over a long time window is preferred in the clinical setting. TSPO is upregulated in activated glial cells across the whole brain for

longer time period. Therefore, TSPO is widely used as the best PET imaging target for neuroinflammatory events in many neurological diseases, and the [^{11}C]PK11195 tracer is well studied for its specificity for inflammation and pharmacokinetics (Chauveau et al., 2008), (Wala et al., 2000). The short half-life of [^{11}C]PK11195 (20 min) hinders widespread clinical use, while the long half-life of [^{123}I]CLINDE (13 h) makes it an attractive tracer for clinical use. In this study, with respect to the reproducibility of CD68-positive microglial distributions; CD68-positive microglial distributions indicated actual inflammation (Zammit et al., 2020), [^{11}C]PK11195-PET and [^{123}I]CLINDE-SPECT images demonstrated equal levels of reproducibility. For instance, both the immunohistochemistry and the PET/SPECT exhibited substantial neuroinflammation at the rim of infarct with less neuroinflammation in the center of infarct in severe cases. To the best of our knowledge, no study has compared [^{11}C]PK11195-PET and [^{123}I]CLINDE-SPECT images, except for one study, in which *ex vivo* autoradiography with [^{123}I]CLINDE was compared with *in vitro* autoradiography with [^{3}H]PK11195 in a rat model with excitotoxic quinolinic acid injection into the striatum (Arlicot et al., 2008). The study reported the relative equivalence between the two tracers (Arlicot et al., 2008).

Either [^{11}C]PK11195 or [^{123}I]CLINDE distributions did not correlate significantly with CD68 staining images in ROIs other than the ROI set for striatum. One of the reasons for this outcome is differences in ischemic tolerances and sensitivities to inflammation among anatomical regions, such as the hippocampus, cerebral cortex, and thalamus. The MCA regions at the striatum and hippocampus levels and the central area at the hippocampus level contained multiple anatomical regions; this might have caused the correlation in those ROIs to be poor. On the other hand, the ROI for striatum included only the striatum; therefore, the correlation in the region were better. Another reason why the correlations between PET/SPECT and immunohistochemistry were not strong is the difference in timings for the PET/SPECT (Day 6) and immunohistochemistry (Day 9). Not only biological features, such as the binding affinity of tracers for the target site but also the accuracy of visualized images must be evaluated in preclinical studies to apply neuroinflammation imaging to clinical practice.

Studies show that CBF and $CMRO_2$ are significantly reduced in the acute phase of ischemic stroke; subsequently, CBF returns to approximately 80% of baseline by 24 hours after onset due to recanalization of the occluded artery or recruitment of collateral pathways, whereas the reduced $CMRO_2$ does not recover even after the reperfusion, especially in the striatum (Giffard et al., 2004) (Lin and Powers, 2018). In line with the literature, CBF measured in the subacute phase (= Day 7) returned to near normal level in some animals and did not correlate with the severity of infarct measured on T2W images. In contrast, the reduction of $CMRO_2$ in the ipsilateral hemisphere was demonstrated on Day 7 in all animals with pMCAo. The reduction in $CMRO_2$ well correlated with the severity of infarct measured on T2W images; the reduction was more obvious in animals with severe infarctions than in animals with moderate to mild infarctions. The reduction of CBV ranges from normal to mild in ischemic stroke in humans (Lin and Liebeskind, 2016). In the rodent brain, due to cross-perfusion from contralateral vessels via a circle of Willis, a remarkable reduction in CBV was not observed.

This study found that the distribution patterns of [^{123}I]CLINDE better reflected the morphological severity of injury confirmed by MRI and H&E-stained brain sections. The distributions of [^{123}I]CLINDE were very similar among the animals with severe infarctions; i.e., marked neuroinflammation in the peri-infarct region and mild neuroinflammation in the ischemic core. This phenomenon is reported in a rat model of pMCAo (Schroeter et al., 2009) and in stroke patients (Price et al., 2006) by [^{11}C]PK11195-PET, although other studies report heterogenous results. In animals with mild infarctions, the accumulation was mainly seen in the striatum. In those with moderate infarctions, the accumulation was both in the striatum and cortex. Although TSPO receptor blocking studies have shown that the binding site of PK11195 and CLINDE is the same (Mattner et al., 2008), (Arlicot et al., 2008), (Arlicot et al., 2010), our [^{123}I]CLINDE-SPECT images tended to better exhibit above-mentioned severity-dependent distribution patterns of neuroinflammation than [^{11}C]PK11195-PET. In contrast, rodent models of transient MCAo with [^{11}C]PK11195 or [18F]DPA714-PET report that inflammatory response is located both in the ischemic core and adjacent area, but to a lesser extent than in the core (Rojas et al., 2007) (Zinnhardt et al., 2015).

Taken together, in the perspective of pathophysiological mechanisms of pMCAo in rodents, the striatum was most susceptible to inflammation, which expand to the cortex and other brain regions, and when the ischemic insult is severe, inflammation occurs mainly in the border region of the infarct.

Neuroinflammation in those regions may have demonstrated that the injury process and possible repair process were in progress. The regions with marked neuroinflammation shown by [^{123}I]CLINDE-SPECT well correlated with regions with mild reduction of $CMRO_2$ demonstrated by ^{15}O-gas PET either in animals with severe infarctions or those with moderate-mild infarctions. A profound reduction in $CMRO_2$ in the ischemic core in severe cases means that there were few viable cells, hence less neuroinflammation, and that the region would be considered to have irrecoverable tissue damage. Regions with mild reduction of the $CMRO_2$ and high neuroinflammation may be salvageable with treatments.

This study has some limitations. The biggest limitation is the lack of quantitative analysis. Many results are presented qualitatively and descriptively, not quantitatively. As Fig. 6 shows, there were large inter-animal variability in each imaging. High signal intensity often expanded several different brain regions, and also, the signal intensities often showed patchy distribution within a single brain region. Moreover, even though a high signal area looked similar in size, such high signal area extended from a half of one brain region to a half of another brain region in one rat, while such high signal area confined to one brain region in another rat. Those inter-animal variability made optimal ROI setting extremely challenging and resulted in obtained quantitative results that differed markedly from visual impressions received from the images. Other limitations include the lack of neuroinflammation imaging at different time points and the lack of long-term outcome in the brain morphology and behaviors.

Conclusions

In this study, [^{123}I]CLINDE-SPECT showed high contrast and specificity for neuroinflammation. [^{123}I]CLINDE-SPECT allows better understand dynamic disease progress in stroke patients. This

neuroinflammation imaging is feasible in clinical practice and would provide physicians with information that could help them diagnose patients more accurately and select appropriate treatment corresponding to disease progression. Moreover, multimodal imaging combining neuroinflammation, oxygen metabolism and MRI provide physicians with comprehensive information for better practice for each patient with stroke.

(main text: 4,861 words)

Acknowledgments

All works were performed at National Cerebral and Cardiovascular Center, Osaka, Japan.

Funding

This project was supported by KAKENHI [grant number xxxxxxxx]; and Institutional Research Fund of National Cerebral and Cardiovascular Research Center, Japan.

CRediT authorship contribution statement

Makiko Ohshima: investigation, data curation, formal analysis, validation, writing-original draft. **Tetsuaki Moriguchi:** investigation, data curation,; **Jun-ichiro Enmi:** investigation, data curation, methodology, visualization. **Hidekazu Kawashima:** investigation, data curation, methodology, visualization. **Kazuhiro Koshino:** investigation, data curation, methodology, visualization. **Tsutomu Zeniya:** investigation, data curation, methodology, visualization. **Masahiro Tsuji:** conceptualization, writing-review & editing. **Hidehiro Iida:** conceptualization, project administration, resources, software, validation, funding acquisition, supervision.

Declaration of competing interest

All authors declare that there is no competing financial interests that could have influenced this study.

Data availability

Data will be made available on request.

Figure legends

Figure 1. (A) Imaging protocols. In Exp. 1, permanent middle cerebral artery occlusion (pMCAo) was induced on Day 0, and magnetic resonance imaging (MRI) and magnetic resonance angiography (MRA) were performed on Days 3-4. [^{11}C]PK11195 positron emission tomography (PET) and [^{123}I]CLINDE single photon emission computed tomography (SPECT) were performed on the same day, Day 6±1. ^{15}O-gas-PET imaging were performed on Day 7±1. After the second MRI on Day 8±1, animals were sacrificed, and their brains were subjected to morphological analysis in hematoxylin and eosin (H&E)-stained sections.) and immunohistochemical analysis in CD68-stained sections. In Exp. 2, [^{123}I]CLINDE autoradiography was performed on Day 6±1 after MRI and MRA on Days 3-4. (B) Representative MRA images, a coronal image (left) and a horizontal image (right) taken on Day 9. Blood flow in the left MCA was blocked after pMCAo. Red arrows indicate the right MCA. (C) Chemical structure of [^{11}C]PK11195. (D) Chemical structure of [^{123}I]CLINDE. (E) ROIs setting for correlation analysis. Subregions of the MCA territory (*a* = striatum; *b* = cortex; *c* = MCA region) were quantified on [^{11}C]PK11195 PET, [^{123}I]CLINDE SPECT, and ^{15}O-gas PET images.

Figure 2. Time-activity curves (TACs) after the injection of radioisotopes. (A, B) TAC of [^{11}C]PK11195. By 10 min after injection, ipsilateral [^{11}C]PK11195 activity was clearly increased compared to contralateral activity at both the striatal and hippocampal levels. (C, D) TAC of [^{123}I]CLINDE. By 10 min after injection, ipsilateral [^{123}I]CLINDE activity was clearly increased compared to contralateral activity at both the striatal and hippocampal levels. ** p <0.01

Figure 3. Comparison of [^{123}I]CLINDE-SPECT, [^{11}C]PK11195-PET, MRI, CD68, and H&E staining images. Representative images in a rat (rat No.1 in Fig. 6). Coronal sections from the frontal pole to the occipital pole are presented from left to right. The signals of [^{123}I]CLINDE and [^{11}C]PK11195 were high in the peri-infarct area, as determined by MRI T2-weighted (T2W) images and H&E staining. High uptake of [^{11}C]PK11195 and [^{123}I]CLINDE , individually, was observed in the area where CD68-positive microglia accumulated.

Figure 4. Correlation analysis between the CD68-positive area and neuroinflammation imaging results: [^{123}I]CLINDE SPECT or [^{11}C]PK11195 PET. The CD68-positive area ratio (%) in the ipsilateral hemisphere and ipsilateral/contralateral radioactivity in each ROI shown in Fig. 1E at the striatum level were plotted. (A) Comparisons of [^{123}I]CLINDE uptake vs. the CD68-positive area. The highest correlation between [^{123}I]CLINDE uptake and CD68-positive microglial accumulation was shown in the striatum. (B) Comparisons of [^{11}C]PK11195 uptake and the CD68-positive area. As with [^{123}I]CLINDE, the best correlation between [^{11}C]PK11195- and CD68-positive microglial accumulation was in the striatum. ** p <0.01, *n.s* = no significance

Figure 5. Representative images of [^{123}I]CLINDE autoradiography in striatal and hippocampal slices. Mild (top row panel) to severe (third row panel) infarcts determined by evaluation of MRI scans are presented, and the control image is shown in the bottom row panel. Animals with a mild infarct (No. 10) showed the most accumulation of [^{123}I]CLINDE in the striatum at the striatal level and very little uptake at the hippocampal level. In animals with a moderate infarct (No. 11), [^{123}I]CLINDE was distributed over a wide region of the MCA territory at both the striatal and hippocampal levels. In animals with a severe infarct (No. 12), a distribution of [^{123}I]CLINDE surrounding the area devoid of the distribution in the ischemic core, i.e., the striatum and overlying cortex was observed, and the distribution extended beyond the MCA region. ARG; autoradiogram, N/A; not available.

Figure 6. [^{123}I]CLINDE-SPECT, [^{11}C]PK11195-PET, ^{15}O-gas PET (cerebral blood flow (CBF): C$^{15}O_2$, cerebral metabolic rate of oxygen ($CMRO_2$): $^{15}O_2$, cerebral blood volume (CBV): C^{15}O), and T2W images at the striatal level in all animals evaluated in Exp. 1. Severity was defined as the infarct size detected on T2W images on Day 8 ± 1. MRI/PET/SPECT images for each animal from severe to moderate infarcts are presented from left to right. [^{123}I]CLINDE uptake in animals with severe infarctions (No. 1-5) was observed in the peri-infarct area on the medial side, whereas that in animals with moderate to mild infarctions (No. 6-9) was observed mostly in the striatum. [^{11}C]PK11195 uptake was observed in the striatum or cortex regardless of the severity. CBF in the ipsilateral hemisphere was decreased in most animals; the decrease, however, did not correspond to the severity. A reduction in the $CMRO_2$ was observed in all animals, and the degree of reduction reflected the severity. CBV alterations were not observed in all animals. T2W images on Day 8 ± 1 showed a clear infarct in the MCA territory in the ipsilateral hemisphere in all animals.

(751 words)

References

Abe, K., Tonomura, M., Ito, M., Takai, N., Imamoto, N., Rokugawa, T., Momosaki, S., Fukumoto, K., Morimoto, K., Inoue, O., 2015. Imaging of reactive oxygen species in focal ischemic mouse brain using a radical trapping tracer [(3)H]hydromethidine. EJNMMI Res 5, 115.

Arlicot, N., Katsifis, A., Garreau, L., Mattner, F., Vergote, J., Duval, S., Kousignian, I., Bodard, S., Guilloteau, D., Chalon, S., 2008. Evaluation of CLINDE as potent translocator protein (18 kDa) SPECT radiotracer reflecting the degree of neuroinflammation in a rat model of microglial activation. European journal of nuclear medicine and molecular imaging 35, 2203-2211.

Arlicot, N., Petit, E., Katsifis, A., Toutain, J., Divoux, D., Bodard, S., Roussel, S., Guilloteau, D., Bernaudin, M., Chalon, S., 2010. Detection and quantification of remote microglial activation in rodent models of focal ischaemia using the TSPO radioligand CLINDE. European journal of nuclear medicine and molecular imaging 37, 2371-2380.

Bambauer, K.Z., Johnston, S.C., Bambauer, D.E., Zivin, J.A., 2006. Reasons why few patients with acute stroke receive tissue plasminogen activator. Archives of neurology 63, 661-664.

Chauveau, F., Boutin, H., Van Camp, N., Dolle, F., Tavitian, B., 2008. Nuclear imaging of neuroinflammation: a comprehensive review of [11C]PK11195 challengers. European journal of nuclear medicine and molecular imaging 35, 2304-2319.

Crawshaw, A.A., Robertson, N.P., 2017. The role of TSPO PET in assessing neuroinflammation. Journal of neurology 264, 1825-1827.

Cumming, P., Burgher, B., Patkar, O., Breakspear, M., Vasdev, N., Thomas, P., Liu, G.J., Banati, R., 2018. Sifting through the surfeit of neuroinflammation tracers. Journal of cerebral blood flow and metabolism : official journal of the International Society of Cerebral Blood Flow and Metabolism 38, 204-224.

Dirnagl, U., Iadecola, C., Moskowitz, M.A., 1999. Pathobiology of ischaemic stroke: an integrated view. Trends in neurosciences 22, 391-397.

Diseases, G.B.D., Injuries, C., 2020. Global burden of 369 diseases and injuries in 204 countries and territories, 1990-2019: a systematic analysis for the Global Burden of Disease Study 2019. Lancet 396, 1204-1222.

Drieu, A., Levard, D., Vivien, D., Rubio, M., 2018. Anti-inflammatory treatments for stroke: from bench to bedside. Ther Adv Neurol Disord 11, 1756286418789854.

Giffard, C., Young, A.R., Kerrouche, N., Derlon, J.M., Baron, J.C., 2004. Outcome of acutely ischemic brain tissue in prolonged middle cerebral artery occlusion: a serial positron emission tomography investigation in the baboon. Journal of cerebral blood flow and metabolism : official journal of the International Society of Cerebral Blood Flow and Metabolism 24, 495-508.

Gonzalez, R.G., 2012. Clinical MRI of acute ischemic stroke. J Magn Reson Imaging 36, 259-271.

Jadhav, A.P., Desai, S.M., Jovin, T.G., 2021. Indications for Mechanical Thrombectomy for Acute Ischemic Stroke: Current Guidelines and Beyond. Neurology 97, S126-S136.

Lambertsen, K.L., Finsen, B., Clausen, B.H., 2019. Post-stroke inflammation-target or tool for therapy? Acta neuropathologica 137, 693-714.

Lin, M.P., Liebeskind, D.S., 2016. Imaging of Ischemic Stroke. Continuum (Minneap Minn) 22, 1399-1423.

Lin, W., Powers, W.J., 2018. Oxygen metabolism in acute ischemic stroke. Journal of cerebral blood flow and metabolism : official journal of the International Society of Cerebral Blood Flow and Metabolism 38, 1481-1499.

Mattner, F., Mardon, K., Katsifis, A., 2008. Pharmacological evaluation of [123I]-CLINDE: a radioiodinated imidazopyridine-3-acetamide for the study of peripheral benzodiazepine binding sites (PBBS). European journal of nuclear medicine and molecular imaging 35, 779-789.

McBride, D.W., Zhang, J.H., 2017. Precision Stroke Animal Models: the Permanent MCAO Model Should Be the Primary Model, Not Transient MCAO. Translational stroke research.

Memezawa, H., Minamisawa, H., Smith, M.L., Siesjo, B.K., 1992. Ischemic penumbra in a model of reversible middle cerebral artery occlusion in the rat. Exp Brain Res 89, 67-78.

Narayanaswami, V., Dahl, K., Bernard-Gauthier, V., Josephson, L., Cumming, P., Vasdev, N., 2018. Emerging PET Radiotracers and Targets for Imaging of Neuroinflammation in Neurodegenerative Diseases: Outlook Beyond TSPO. Mol Imaging 17, 1536012118792317.

Olmez, I., Ozyurt, H., 2012. Reactive oxygen species and ischemic cerebrovascular disease. Neurochemistry international 60, 208-212.

Powers, W.J., Rabinstein, A.A., Ackerson, T., Adeoye, O.M., Bambakidis, N.C., Becker, K., Biller, J., Brown, M., Demaerschalk, B.M., Hoh, B., Jauch, E.C., Kidwell, C.S., Leslie-Mazwi, T.M., Ovbiagele, B., Scott, P.A., Sheth, K.N., Southerland, A.M., Summers, D.V., Tirschwell, D.L., 2019. Guidelines for the Early Management of Patients With Acute Ischemic Stroke: 2019 Update to the 2018 Guidelines for the Early Management of Acute Ischemic Stroke: A Guideline for Healthcare Professionals From the American Heart Association/American Stroke Association. Stroke; a journal of cerebral circulation 50, e344-e418.

Price, C.J., Wang, D., Menon, D.K., Guadagno, J.V., Cleij, M., Fryer, T., Aigbirhio, F., Baron, J.C., Warburton, E.A., 2006. Intrinsic activated microglia map to the peri-infarct zone in the subacute phase of ischemic stroke. Stroke; a journal of cerebral circulation 37, 1749-1753.

Rojas, S., Martin, A., Arranz, M.J., Pareto, D., Purroy, J., Verdaguer, E., Llop, J., Gomez, V., Gispert, J.D., Millan, O., Chamorro, A., Planas, A.M., 2007. Imaging brain inflammation with [(11)C]PK11195 by PET and induction of the peripheral-type benzodiazepine receptor after transient focal ischemia in rats. Journal of cerebral blood flow and metabolism : official journal of the International Society of Cerebral Blood Flow and Metabolism 27, 1975-1986.

Saqqur, M., Molina, C.A., Salam, A., Siddiqui, M., Ribo, M., Uchino, K., Calleja, S., Garami, Z., Khan, K., Akhtar, N., O'Rourke, F., Shuaib, A., Demchuk, A.M., Alexandrov, A.V., Investigators, C., 2007. Clinical deterioration after intravenous recombinant tissue plasminogen activator treatment: a multicenter transcranial Doppler study. Stroke; a journal of cerebral circulation 38, 69-74.

Schroeter, M., Dennin, M.A., Walberer, M., Backes, H., Neumaier, B., Fink, G.R., Graf, R., 2009. Neuroinflammation extends brain tissue at risk to vital peri-infarct tissue: a double tracer [11C]PK11195- and [18F]FDG-PET study. Journal of cerebral blood flow and metabolism : official journal of the International Society of Cerebral Blood Flow and Metabolism 29, 1216-1225.

Shah, F., Hume, S.P., Pike, V.W., Ashworth, S., McDermott, J., 1994. Synthesis of the enantiomers of [N-methyl-11C]PK 11195 and comparison of their behaviours as radioligands for PK binding sites in rats. Nucl Med Biol 21, 573-581.

Shimochi, S., Keller, T., Kujala, E., Khabbal, J., Rajander, J., Loyttyniemi, E., Solin, O., Nuutila, P., Kanaya, S., Yatkin, E., Gronroos, T.J., Iida, H., 2022. Evaluation of [(18)F]F-DPA PET for Detecting Microglial Activation in the Spinal Cord of a Rat Model of Neuropathic Pain. Molecular imaging and biology : MIB : the official publication of the Academy of Molecular Imaging 24, 641-650.

Stroke Therapy Academic Industry, R., 1999. Recommendations for standards regarding preclinical neuroprotective and restorative drug development. Stroke; a journal of cerebral circulation 30, 2752-2758.

Temma, T., Yamazaki, M., Miyanohara, J., Shirakawa, H., Kondo, N., Koshino, K., Kaneko, S., Iida, H., 2017. Sequential PET estimation of cerebral oxygen metabolism with spontaneous respiration of (15)O-gas in mice with bilateral common carotid artery stenosis. Journal of cerebral blood flow and metabolism : official journal of the International Society of Cerebral Blood Flow and Metabolism 37, 3334-3343.

Wala, E.P., Sloan, J.W., Jing, X., 2000. Pharmacokinetics of the peripheral benzodiazepine receptor antagonist, PK 11195, in rats. The effect of dose and gender. Pharmacological research 41, 461-468.

Zammit, M., Tao, Y., Olsen, M.E., Metzger, J., Vermilyea, S.C., Bjornson, K., Slesarev, M., Block, W.F., Fuchs, K., Phillips, S., Bondarenko, V., Zhang, S.C., Emborg, M.E., Christian, B.T., 2020. [(18)F]FEPPA PET imaging for monitoring CD68-positive microglia/macrophage neuroinflammation in nonhuman primates. EJNMMI Res 10, 93.

Zinnhardt, B., Viel, T., Wachsmuth, L., Vrachimis, A., Wagner, S., Breyholz, H.J., Faust, A., Hermann, S., Kopka, K., Faber, C., Dolle, F., Pappata, S., Planas, A.M., Tavitian, B., Schafers, M., Sorokin,

L.M., Kuhlmann, M.T., Jacobs, A.H., 2015. Multimodal imaging reveals temporal and spatial microglia and matrix metalloproteinase activity after experimental stroke. Journal of cerebral blood flow and metabolism : official journal of the International Society of Cerebral Blood Flow and Metabolism 35, 1711-1721.

Figure 1 (1.5-column fitting image)

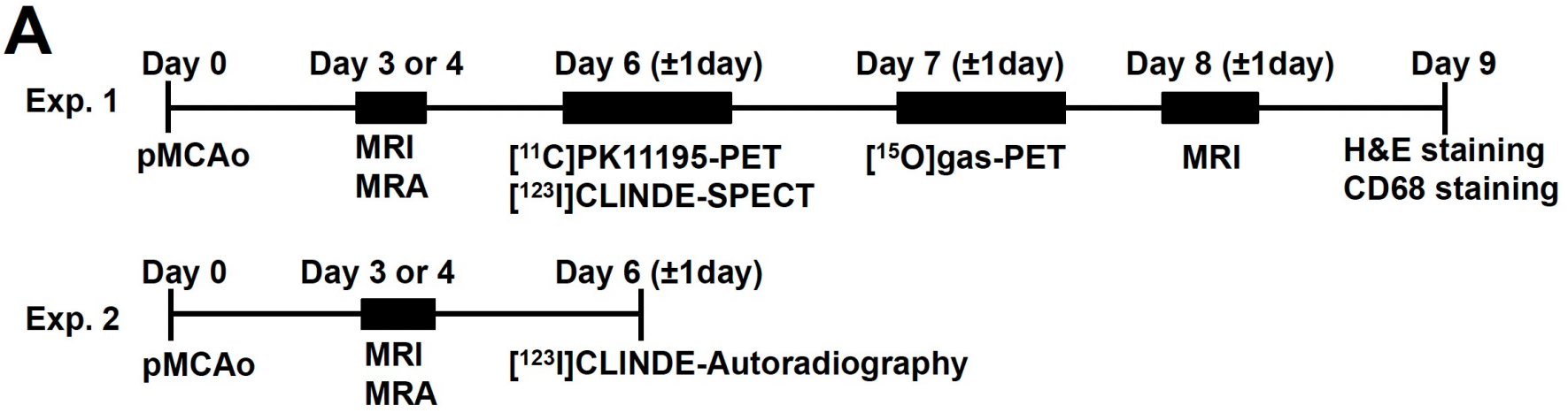

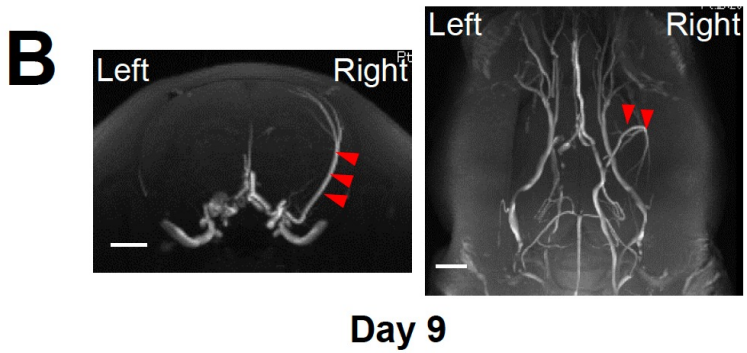

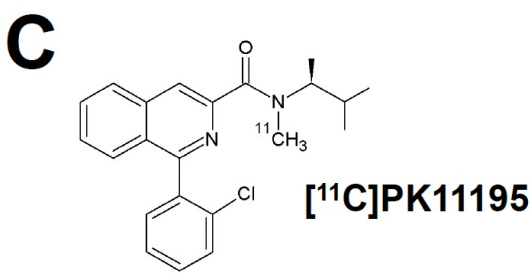

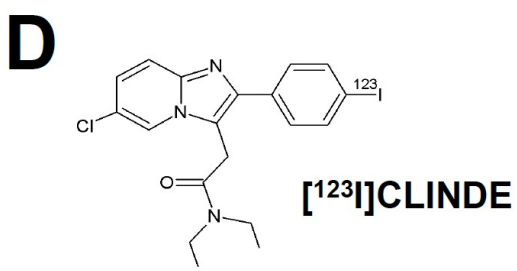

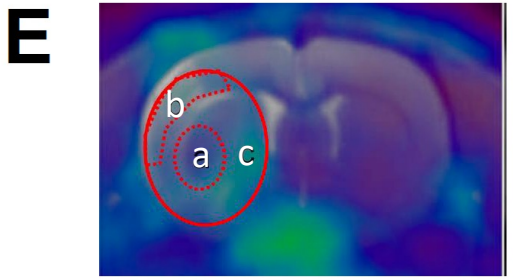

Figure 2 (single-column fitting image)

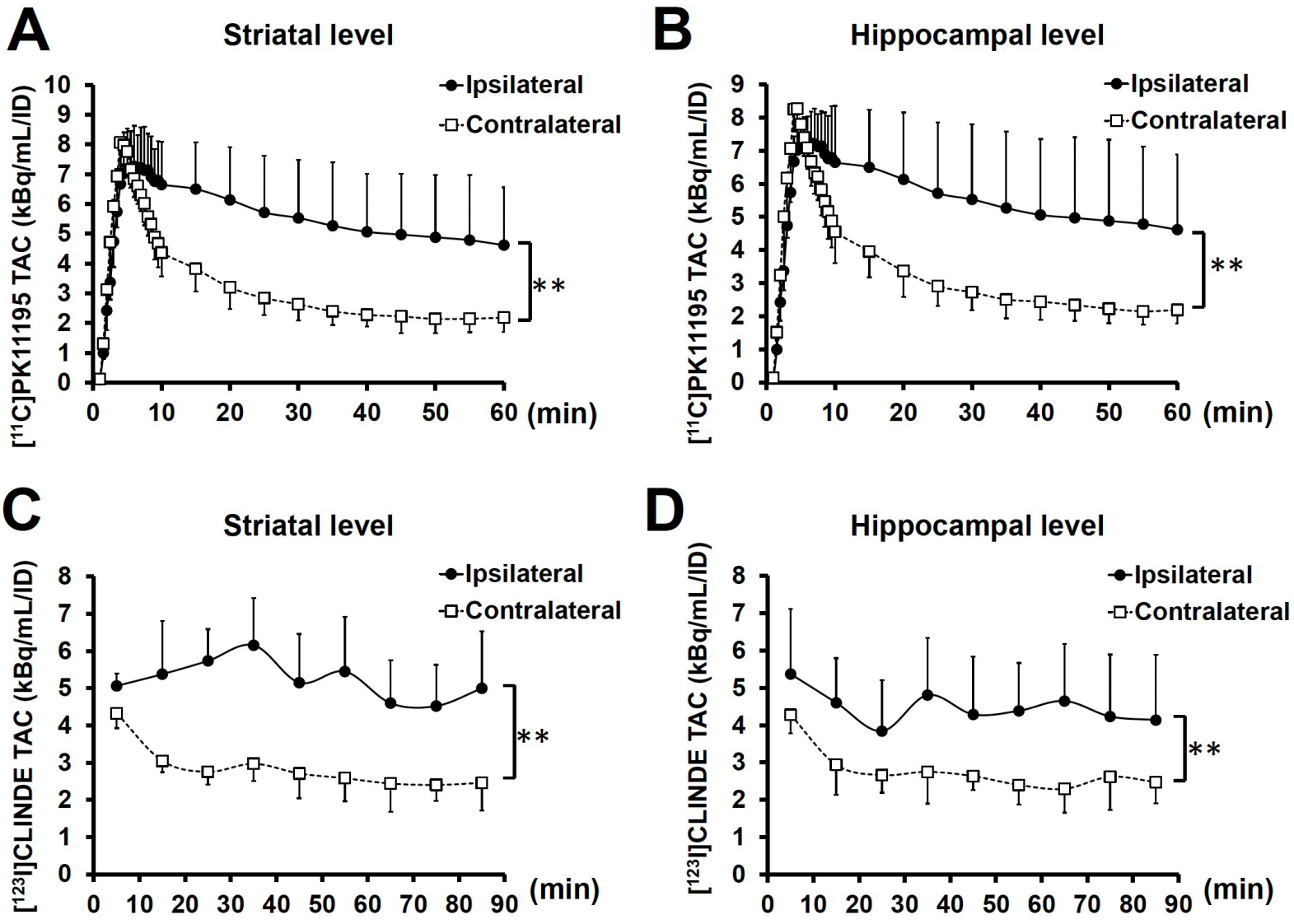

Figure 3 (2-column fitting image)

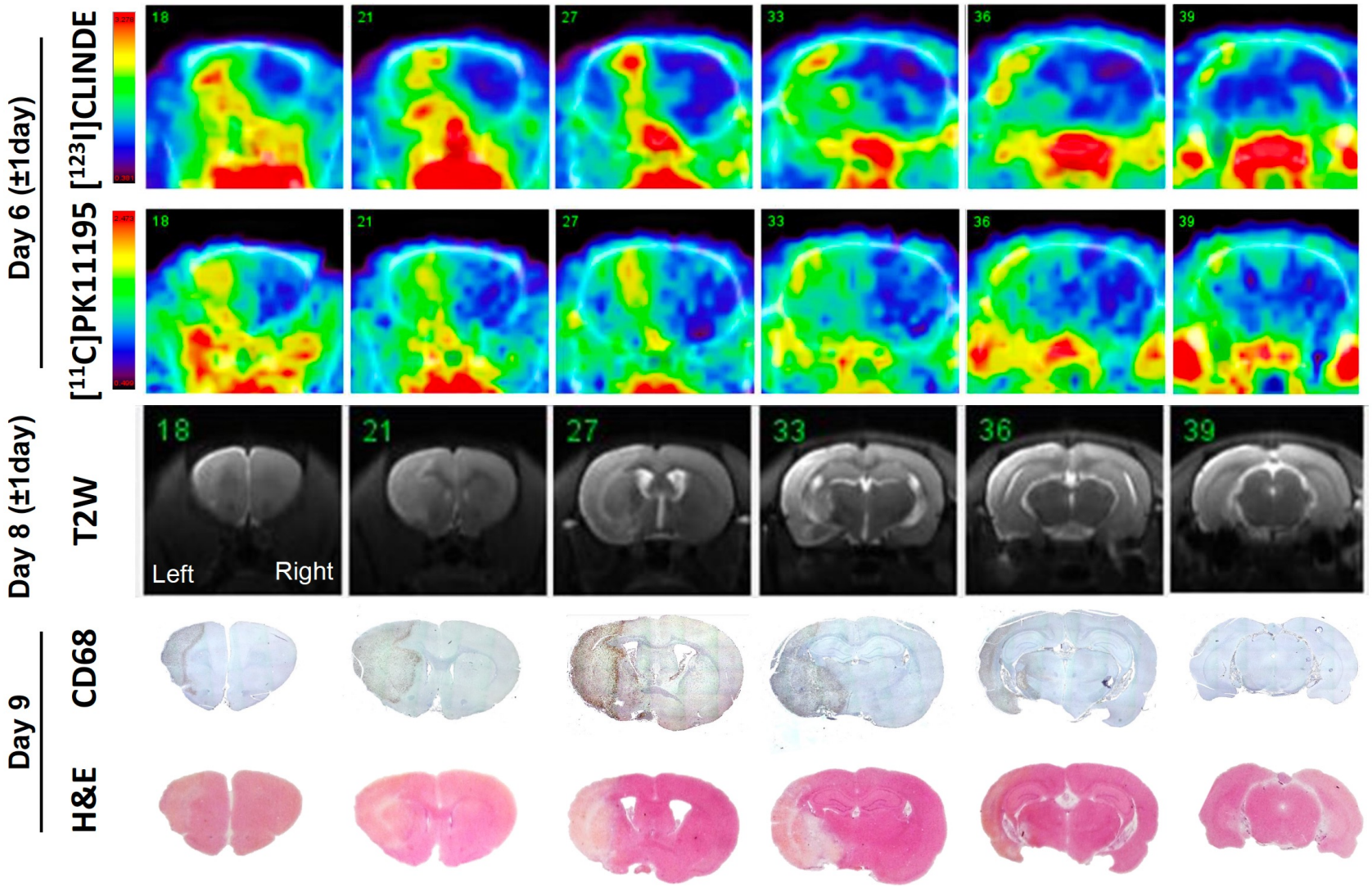

Figure 4 (single-column fitting image)

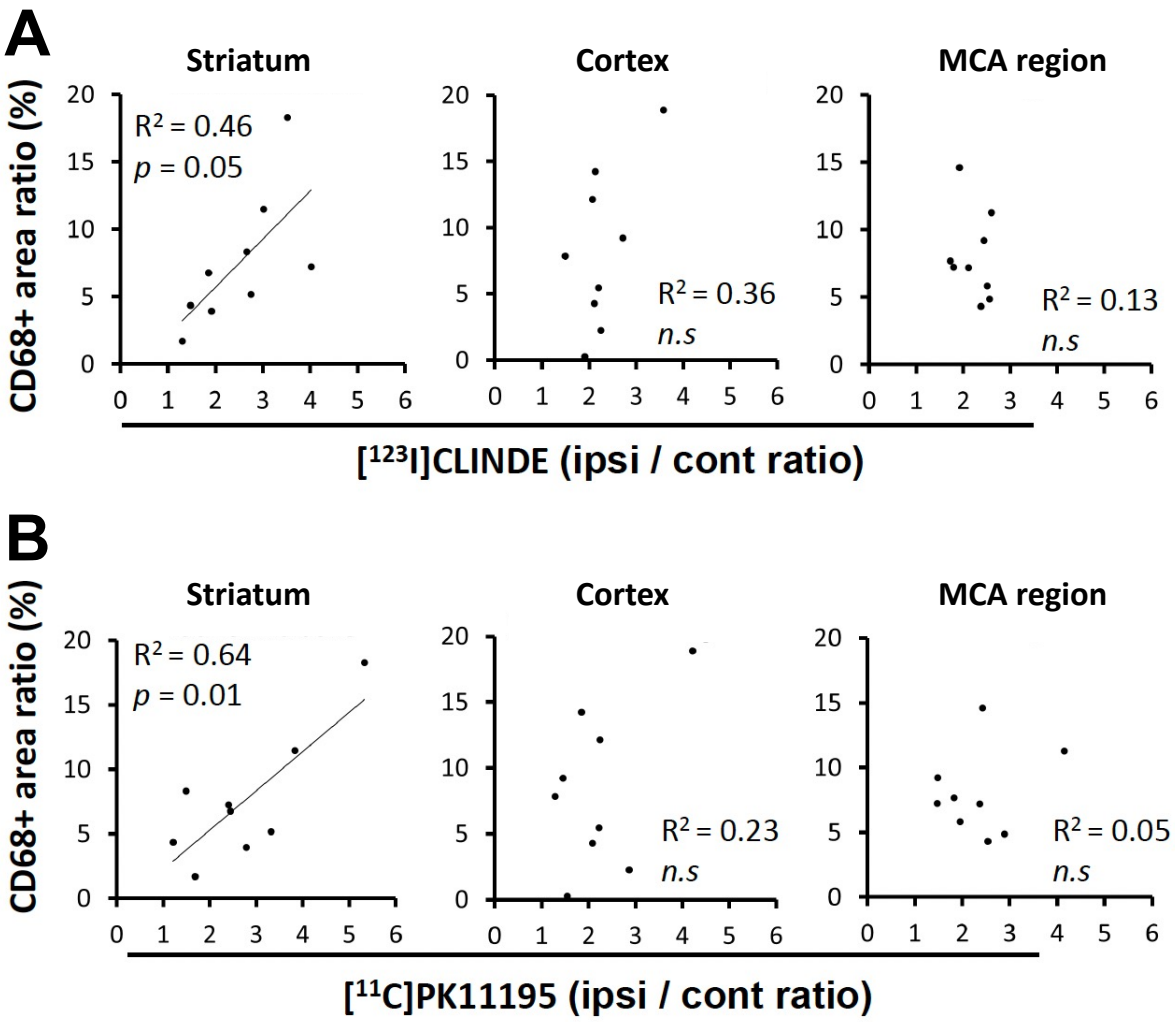

Figure 5 (1.5-column fitting image)

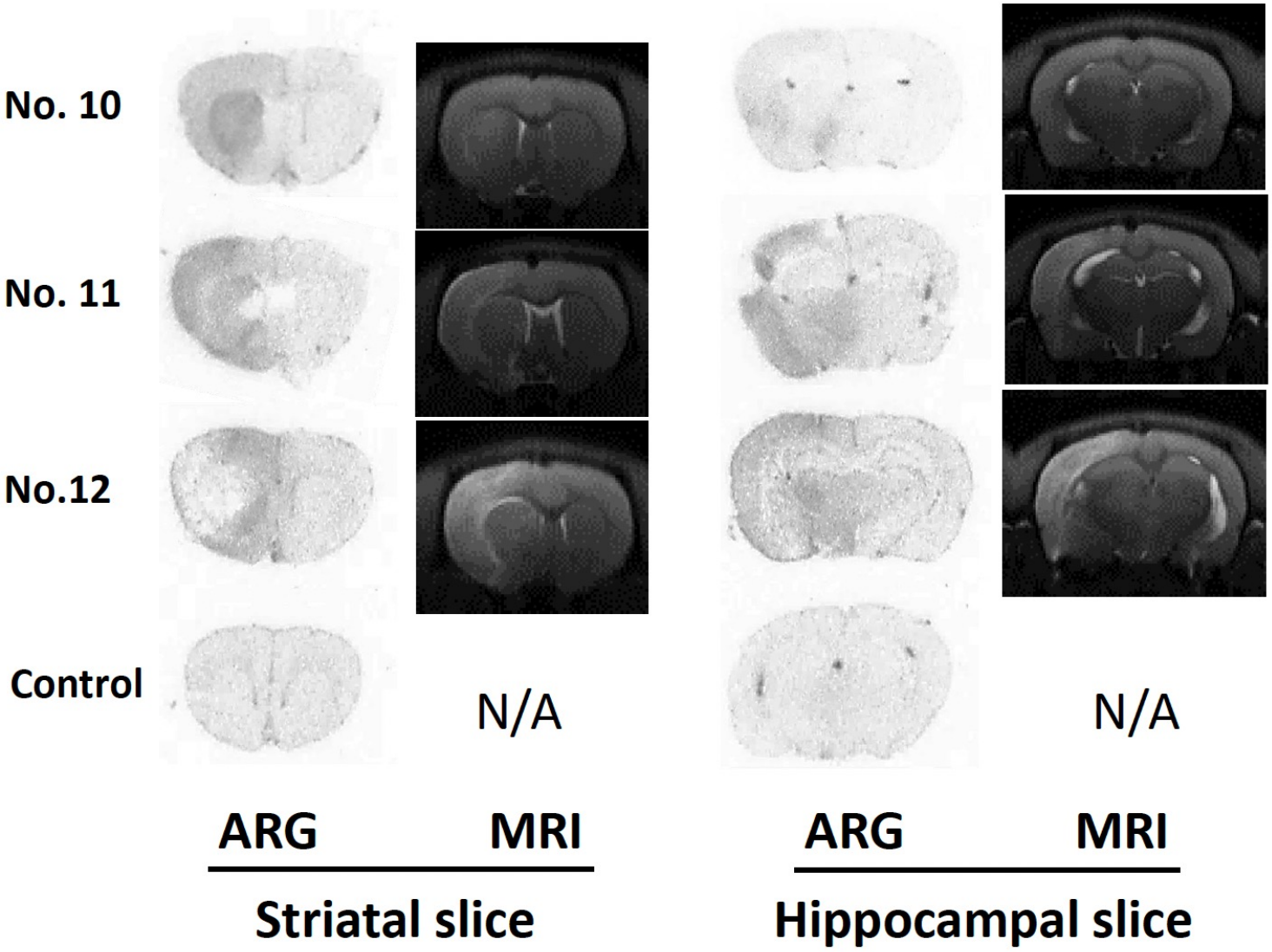

Figure 6 (2-column fitting image)